

1 **Satellite-based Estimation of the Impacts of Summertime Wildfires on**
2 **PM_{2.5} concentration in United States**

3 **Zhixin Xue¹, Pawan Gupta^{2,3}, and Sundar Christopher¹**

4 ¹Department of Atmospheric and Earth Science, The University of Alabama in Huntsville,
5 Huntsville, 35806 AL, USA

6 ²STI, Universities Space Research Association (USRA), Huntsville, 35806 AL, USA

7 ³NASA Marshall Space Flight Center, Huntsville, AL, 35806, USA

8 **Abstract**

9 Frequent and widespread wildfires in North Western United States and Canada has become
10 the “*new normal*” during the northern hemisphere summer months, which significantly degrades
11 particulate matter air quality in the United States. Using the mid-visible Multi Angle
12 Implementation of Atmospheric Correction (MAIAC) satellite-derived Aerosol Optical Depth
13 (AOD) with meteorological information from the European Centre for Medium-Range Weather
14 Forecasts (ECMWF) and other ancillary data, we quantify the impact of these fires on fine
15 particulate matter concentration (PM_{2.5}) air quality in the United States. We use a Geographically
16 Weighted Regression method to estimate surface PM_{2.5} in the United States between low (2011)
17 and high (2018) fire activity years. Our results indicate that smoke aerosols caused significant
18 pollution changes over half of the United States. We estimate that nearly 29 states have increased
19 PM_{2.5} during the fire active year and 15 of these states have PM_{2.5} concentrations more than 2
20 times than that of the inactive year. Furthermore, these fires increased the daily mean surface PM_{2.5}
21 concentrations in Washington and Oregon by 38 to 259µgm⁻³ posing significant health risks
22 especially to vulnerable populations. Our results also show that the GWR model can be

23 successfully applied to PM_{2.5} estimations from wildfires thereby providing useful information for
24 various applications including public health assessment.

25 **1. Introduction**

26 The United States (US) Clean Air Act (CAA) was passed in 1970 to reduce pollution levels
27 and protect public health that has led to significant improvements in air quality (Hubbell et al.,
28 2010; Samet, 2011). However, the northern part of the US continues to experience an increase in
29 surface PM_{2.5} due to fires in North Western United States and Canada (hereafter NWUSC)
30 especially during the summer months and these aerosols are a new source of ‘pollution’ (Coogan
31 et al., 2019; Dreessen et al., 2016). The smoke aerosols from these fires increase fine particulate
32 matter (PM_{2.5}) concentrations and degrade air quality in the United States (Miller et al., 2011).
33 Moreover several studies have shown that from 2013 to 2016, over 76% of Canadians and 69% of
34 Americans were at least minimally affected by wildfire smoke (Munoz-Alpizar et al., 2017).
35 Although wildfire pre-suppression and suppression costs have increased, the number of large fires
36 and the burnt areas in many parts of western Canada and the United States have also increased.
37 (Hanes et al., 2019; Tymstra et al., 2019). Furthermore, in a changing climate, as surface
38 temperature increases and humidity decreases, the flammability of land cover also increases, and
39 thus accelerate the spread of wildfires (Melillo et al., 2014). The accumulation of flammable
40 materials like leaf litter can potentially trigger severe wildfire events even in those forests that
41 hardly experience wildfires (Calkin et al., 2015; Hessburg et al., 2015; Stephens, 2005).

42 Wildfire smoke exposure can cause small particles to be lodged in lungs that may lead to
43 exacerbations of asthma chronic obstructive pulmonary disease (COPD), bronchitis, heart disease
44 and pneumonia (Apte et al., 2018; Cascio, 2018). According to a recent study, a 10 $\mu\text{g m}^{-3}$
45 increase in PM_{2.5} is associated with a 12.4% increase in cardiovascular mortality (Kollanus et al.,

46 2016). In addition, exposure to wildfire smoke is also related to massive economic costs due to
47 premature mortality, loss of workforce productivity, impacts on the quality of life and
48 compromised water quality (Meixner and Wohlgemuth, 2004).

49 Surface $PM_{2.5}$ is one of the most commonly used parameters to assess the health effects of
50 ambient air pollution. Given the sparsity of measurements in many parts of the world, it is not
51 possible to use interpolation techniques between monitors to provide $PM_{2.5}$ estimates on a square
52 kilometer basis. Since surface monitors are limited, satellite data has been used with numerous
53 ancillary data sets to estimate surface $PM_{2.5}$ at various spatial scales. Several techniques have been
54 developed to estimate surface $PM_{2.5}$ using satellite observations from regional to global scales
55 including simple linear regression, multiple linear regression, mixed-effect model, chemical
56 transport model (scaling methods), geographically weighted regression (GWR), and machine
57 learning methods (see Hoff and Christopher, 2009 for a review). The commonly used global
58 satellite data product is the 550nm (mid-visible) aerosol optical depth (AOD) which is a unitless
59 columnar measure of aerosol extinction. Simple linear regression method uses satellite AOD as
60 the only independent variable, which shows limited predictability compared to other methods and
61 correlation coefficients vary from 0.2 to 0.6 from the Western to Eastern United States (Zhang et
62 al., 2009). Multiple linear regression method uses meteorological variables along with AOD data,
63 and the prediction accuracy varies with different conditions including the height of boundary layer
64 and other meteorological conditions (Goldberg et al., 2019; Gupta and Christopher, 2009b; Liu et
65 al., 2005). For both univariate model and multi-variate models, AOD shows stronger correlation
66 with $PM_{2.5}$ during-fire episodes compared to pre-fire and post-fire periods (Mirzaei et al., 2018).
67 Chemistry transport models (CTM) that scale the satellite AOD by the ratio of $PM_{2.5}$ to AOD
68 simulated by models can provide $PM_{2.5}$ estimations without ground measurements, which are

69 different than other statistical methods (Donkelaar et al., 2019, 2006). However, the CTM models
70 that depend on reliable emission data usually show limited predictability at shorter time scales,
71 and is largely useful for studies that require annual averages (Hystad et al., 2012).

72 The relationship among $PM_{2.5}$, AOD and other meteorological variables is not spatially
73 consistent (Hoff and Christopher, 2009; Hu, 2009). Therefore, methods that consider spatial
74 variability can replicate surface $PM_{2.5}$ with higher accuracy. One such method is the GWR, which
75 is a non-stationary technique that models spatially varying relationships by assuming that the
76 coefficients in the model are functions of locations (Brunsdon et al., 1996; Fotheringham et al.,
77 1998, 2003). In 2009, satellite-retrieved AOD was introduced in the GWR method to predict
78 surface $PM_{2.5}$ (Hu, 2009) followed by the use of meteorological parameters and land use
79 information (Hu et al., 2013). Meteorological variables are crucial for simulating surface $PM_{2.5}$
80 since they interact with $PM_{2.5}$ through different processes which will be discussed in detail in the
81 data section (Chen et al., 2020). Several studies (Guo et al., 2021; Ma et al., 2014; You et al.,
82 2016) successfully applied the GWR model in estimating $PM_{2.5}$ in China by using AOD and
83 meteorological features as predictors. Similar to all the statistical methods, however, the GWR
84 relies on adequate number and density of surface measurements (Chu et al., 2016; Gu, 2019; Guo
85 et al., 2021), underscoring the importance of adequate ground monitoring of surface $PM_{2.5}$.

86 In this paper, we use satellite data from the Moderate Resolution Imaging
87 Spectroradiometer (MODIS) and surface $PM_{2.5}$ data combined with meteorological and other
88 ancillary information to develop and use the GWR method to estimate $PM_{2.5}$. The use of the GWR
89 method is not novel and we merely use a proven method to estimate surface $PM_{2.5}$ from forest
90 fires. We calculate the change in $PM_{2.5}$ between a high fire activity (2018) with low fire activity
91 (2011) periods during summer to assess the role of NWUSC wildfires on surface $PM_{2.5}$ in the

92 United States. The paper is organized as follows: We describe the data sets used in this study
93 followed by the GWR method. We then describe the results and discussion followed by a summary
94 with conclusions.

95

96 **2. Data**

97 A 17-day period (August 9th to August 25th) in 2018 (high fire activity) and 2011 (low fire
98 activity) was selected based on analysis of total fires (details in methodology section) to assess
99 surface PM_{2.5} (Table 1).

100 **2.1 Ground level PM_{2.5} observations:** Daily surface PM_{2.5} from the Environment Protection
101 Agency (EPA) are used in this study. These data are from Federal Reference Methods (FRM),
102 Federal Equivalent Methods (FEM), or other methods that are to be used in the National Ambient
103 Air Quality Standards (NAAQS) decisions. A total of 1003 monitoring sites in the US are included
104 in our study with 949 having valid observations in the study period in 2018, and a total of 873 sites
105 with 820 having valid observations in the study period in 2011. PM_{2.5} values less than 2 μgm⁻³ are
106 discarded since they are lower than the established detection limit (Hall et al., 2013).

107 **2.2 Satellite Data:** AOD which represents the total column aerosol mass loading is related to
108 surface PM_{2.5} as a function of aerosol vertical properties and physical properties (Koelemeijer et
109 al., 2006):

$$110 \quad AOD = PM_{2.5} H f(RH) \frac{3Q_{ext,dry}}{4\rho r_{eff}} = PM_{2.5} H S \quad (1)$$

111 Where H is the aerosol layer height, f(RH) is the ratio of ambient and dry extinction
112 coefficients, Q_{ext,dry} is the extinction efficiency under dry conditions, r_{eff} is the particle effective

113 radius, ρ is the aerosol mass density and S is the specific extinction efficiency ($\text{m}^2 \text{g}^{-1}$) of the
114 aerosol at ambient conditions. Therefore AOD usually has a strong positive correlation with $\text{PM}_{2.5}$,
115 and the relationship varies depending on other meteorological parameters which will be discussed
116 in detail in the following section.

117 The MODIS mid visible AOD from the Multi-Angle Implementation of Atmospheric
118 Correction (MAIAC) product (MCD19A2 Version 6 data product) is used in this study. We used
119 the MAIAC- retrieved Terra and Aqua MODIS AOD product at 1 km pixel resolution (Lyapustin
120 et al., 2018). Different orbits are averaged to obtain mean daily values. Since thick smoke plumes
121 generated by wildfires can be misclassified as cloud, we preserve possible cloud contaminated
122 pixels to preserve the thick smoke pixels, and only AOD less than 0 will be discarded. Validation
123 with AERONET studies show that 66% of the MAIAC AOD data agree within $\pm 0.5 \sim \pm 0.1$ AOD
124 (Lyapustin et al., 2018). Largely due to cloud cover, grid cells may have limited number of AOD
125 observations within a certain period. On average, cloud free AOD data are available about 40% of
126 the time during August 9th to August 25th in 2018 when fires were active in the region bounded by
127 25~50°N, 65~125°W. Smoke flag from the same product is used as a predictor in estimating
128 surface $\text{PM}_{2.5}$. The smoke detection is performed using MODIS red, blue and deep blue bands, and
129 smoke pixels are separated from dust and clouds based on absorption parameter, size parameter
130 and thermal thresholds (see Lyapustin et al., 2012; 2018 for further discussion). Smoke flag data
131 can provide the percentage of smoke pixel in each grid, which is related to smoke coverage.

132 We also use the MODIS level-3 daily FRP (MCD14ML, fire radiative power) product
133 which combines Terra and Aqua fire products to assess wildfire activity. The fire radiative energy
134 indicates the rate of combustion and thus FRP can be used for characterizing active fires (Freeborn

135 et al, 2014). For purposes of the study we sum the FRP within every $2.3^{\circ}\times 3.5^{\circ}$ box to represent
136 the total fire activity in different locations.

137 **2.3 Meteorological data:** Meteorological information including boundary layer height (BLH), 2m
138 temperature (T2M), 10m wind speed (WS), surface relative humidity (RH) and surface pressure
139 (SP) are obtained from the European Centre for Medium-Range Weather Forecasts (ECMWF)
140 reanalysis (ERA5) product, with a spatial resolution of 0.25 degrees and temporal resolution of 1
141 hour and is matched temporally with the satellite overpass time. The meteorological parameters
142 provide important information of different processes affecting surface $PM_{2.5}$ concentration, which
143 can also be seen as supplements of the AOD- $PM_{2.5}$ relationship as previously discussed.

144 The BLH can provide information of aerosol layer height (H in equation 1) as aerosols are often
145 found to be well-mixed within the boundary layer (Gupta and Christopher, 2009b). With same
146 amount of pollution within the boundary layer, the higher the BLH is, the more $PM_{2.5}$ is distributed
147 within that layer and vice-versa (Miao et al., 2018; Zheng et al., 2017). Therefore, $PM_{2.5}$ usually
148 has an anticorrelation with BLH. However, for wildfire events, the aerosol layer height is
149 sometimes higher than the BLH (Haarig et al., 2018), which leads to lower correlation between
150 AOD and $PM_{2.5}$ since we use only BLH to present the aerosol layer height. Thus BLH can provide
151 aerosol vertical information in most cases except for suspended high-layer aerosol caused by fires,
152 which leads to higher bias of the model for high-layer aerosols near the fire sources. Surface
153 temperature (T2M) can affect $PM_{2.5}$ through convection, evaporation, temperature inversion and
154 secondary pollutants generation processes (Chen et al., 2020). The first two processes are
155 negatively related to $PM_{2.5}$ concentration: 1) higher temperature increases turbulence and
156 atmospheric convections which accelerate the pollution dispersion ($PM_{2.5}$ decreases); 2) higher
157 temperature increases evaporation loss of $PM_{2.5}$ including ammonium nitrate and other volatile or

158 semi-volatile components (Wang et al., 2017). The later two processes are positively related to PM_{2.5}
159 by limiting vertical motion and promoting photochemical reactions under high temperature (Xu et
160 al., 2019; Zhang et al., 2015). Wind speed (WS) are often negatively related to PM_{2.5} since it
161 increases the dispersion of pollutants. However, unique geographical conditions (such like
162 mountains) with certain wind directions can cause accumulations of pollutants (Chen et al., 2017).
163 RH may promote hygroscopic growth of particles to increase PM_{2.5} (Trueblood et al., 2018; Zheng
164 et al., 2017), but it can also reduce PM_{2.5} through the deposition process. SP may influence the
165 diffusion or accumulation of pollutants through formation of low-level wind convergence (You et
166 al., 2017).

167 **3. Methodology**

168 To assess the impact of NWUSC fires on PM_{2.5} in the United States, we first estimate the
169 PM_{2.5} over the study region during a time period with high fire activity (2018). We then use the
170 same method during a year with low fire activity (2011) to compare the differences between the
171 two years. The two years are selected based on the total FRP in August calculated within Canada
172 (49~60°N, 55~135°W) and Northwestern (NW) US (35~49°N, 105~125°W). Table 2 shows the
173 total FRP in Canada and Northwestern US in August from 2010 to 2018. The total FRP in the two
174 regions is lowest in 2011 and highest in 2018 during the 9 years, which provides the basis for the
175 study. In order to create a 0.1° surface PM_{2.5}, the GWR model is used to estimate the relationships
176 of PM_{2.5} and AOD. Detailed processing steps for GWR model are shown in Figure 1.

177 **3.1 Data preprocessing:** The first step is to resample all datasets to a uniform spatial resolution
178 by creating a 0.1° resolution grid covering the Continental United States. During this process, we
179 collocate the PM_{2.5} data and average the values if there is more than one value in one grid. Then

180 the MAIAC AOD and smoke flagare averaged into 0.1° grid cells. Meteorological datasets are
181 also resampled to the 0.1° grid cells by applying the inverse distance method.

182 **3.2 Time selecting & averaging:** Next we select data where AOD and ground $PM_{2.5}$ are both
183 available ($AOD > 0$ and $PM_{2.5} > 2.0 \mu g m^{-3}$) and average them for the study period. This is to
184 ensure that the AOD, $PM_{2.5}$ and other variables match with each other, because $PM_{2.5}$ is not a
185 continuous measurement for some sites and AOD have missing values due to cloud cover and
186 other reasons. Therefore, it is important to use data from days where both measurements are
187 available to avoid sampling biases.

188 **3.3 GWR model development and validation:** The Adaptive bandwidth selected by the Akaike's
189 Information Criterion (AIC) is used for the GWR model (Loader, 1999). For locations that already
190 have $PM_{2.5}$ monitors, we calculate the mean AOD of a $0.5 \times 0.5^\circ$ box centered at the ground location
191 and estimate the GWR coefficients (β) for AOD and meteorological variables to estimate $PM_{2.5}$.
192 The model structure can be expressed as:

$$193 \quad PM_{2.5i} = \beta_{0,i} + \beta_{1,i}AOD_i + \beta_{2,i}BLH_i + \beta_{3,i}T2M_i + \beta_{4,i}U10M_i + \beta_{5,i}RH_{sfci} + \beta_{6,i}SP_i + \beta_{7,i}SF_i \\ 194 \quad \quad \quad + \varepsilon_i$$

195 where $PM_{2.5i}$ ($\mu g m^{-3}$) is the selected ground-level $PM_{2.5}$ concentration at location i ; $\beta_{0,i}$
196 is the intercept at location i ; $\beta_{1,i} \sim \beta_{8,i}$ are the location-specific coefficients; AOD_i is the resampled
197 AOD selected from MAIAC daily AOD data at location i ; $BLH_i, T2M_i, U10M_i, RH_{sfci}, SP_i$ are
198 selected meteorological parameters (BLH, T2M, WS, RH and PS) at location i ; SF_i (%) is the
199 resampled smoke flag data at location i and ε_i is the error term at location i .

200 We perform the Leave One Out Cross Validation (LOOCV) to test the model predictive
201 performance (Kearns and Ron, 1999). Since the GWR model relies on adequate number of

202 observations, the prediction accuracy will be lower if we preserve too much data for validation.
203 Therefore, we choose the LOOCV method, which preserve only one data for validation at a time
204 and repeat the process until all the data are used. In addition, R^2 and RMSE are calculated for both
205 model fitting and model validation process to detect overfitting. Model overfitting will lead to low
206 predictability, which means it fits too close to the limited number of data to predict for other places
207 and will cause large bias.

208 **3.4 Model prediction:** While predicting the ground-level $PM_{2.5}$ for unsampled locations, we make
209 use of the estimated parameters for sites within a 5° radius to generate new slopes for independent
210 variables based on the spatial weighting matrix (Brunsdon et al., 1996). The closer to the predicted
211 location, the closer to 1 the weighting factor will be, while the weighting factor for sites further
212 than the 5° in distance is zero. It is important to note that AOD and other independent variables
213 used for prediction in this step are averaged values for days that have valid AOD, which is different
214 from the data used in the fitting process since $PM_{2.5}$ is not measured every day in all locations.

215 **4. Results and Discussion**

216 We first discuss the surface $PM_{2.5}$ for a few select locations that are impacted by fires
217 followed by the spatial distribution of MODIS AOD and the FRP for August 2018. We then assess
218 the spatial distribution of surface $PM_{2.5}$ from the GWR method. The validation of the GWR method
219 is then discussed. To further demonstrate the impact of the NWUSC fires on $PM_{2.5}$ air quality in
220 the United States, we show the spatial distribution of the difference between August 2018 and
221 August 2011. We further quantify these results for ten US EPA regions.

222 **4.1 Descriptive statistics of satellite data and ground measurements**

223 The 2018 summertime Canadian wildfires started around the end of July in British
224 Columbia and continued until mid-September. The fires spread rapidly to the south of Canada
225 during August, causing high concentrations of smoke aerosols to drift down to the US and affecting
226 particulate matter air quality significantly. From late July to mid-September, wildfires in the
227 northwest US that burnt forest and grassland also affected air quality. Starting with the Cougar
228 Creek Fire, then Crescent Mountain and Gilbert Fires, different wildfires in in NWUSC caused
229 severe air pollution in various US cities. Figure 2a shows the rapid increase in PM_{2.5} of selected
230 US cities from July 1st to August 31st, due to the transport of smoke from these wildfires. For all
231 sites, July had low PM_{2.5} concentrations ($<10 \mu\text{g m}^{-3}$) and rapidly increases as fire activity
232 increases. Calculating only from the EPA ground observations, the mean PM_{2.5} of the 17 days for
233 the whole US is $13.7 \mu\text{g m}^{-3}$ and the mean PM_{2.5} for Washington (WA) is $40.6 \mu\text{g m}^{-3}$, which
234 indicates that the PM pollution is concentrated in the northwestern US for these days. This trend
235 is obvious when comparing the mean PM_{2.5} of all US stations (black line with no markers) and the
236 mean PM_{2.5} of all WA stations (grey line with no markers). Ground-level PM_{2.5} reaches its peak
237 between August 17th-21st and daily PM_{2.5} values during this time period far exceeds the 17-day
238 mean PM_{2.5}. For example, mean PM_{2.5} in WA on August 20th is $86.75 \mu\text{g m}^{-3}$, which is more
239 than two times the 17-day average of this region. On August 19th, Omak which is located in the
240 foothills of the Okanogan Highlands in WA had PM_{2.5} values exceed $250 \mu\text{g m}^{-3}$. According to
241 a review of US wildfire caused PM_{2.5} exposures, 24-h mean PM_{2.5} concentrations from wildfires
242 ranged from 8.7 to $121 \mu\text{g m}^{-3}$, with a 24 h maximum concentration of $1659 \mu\text{g m}^{-3}$ (Navarro et
243 al., 2018).

244 Table 3 shows relevant statistics of 15 states that have at least one daily record of non-
245 attainment of EPA standard ($>35 \mu\text{g m}^{-3}$). From the frequency records of non attainment in the

246 17-day period (last column), four states (Montana, Washington, California and Idaho) were
247 consistently affected by the wildfires, and large portion of ground stations in these states were
248 influenced by smoke aerosols. Most of the neighboring states also suffered from short-term but
249 broad air pollution (third column). Noticeable from these records is that the total number of ground
250 stations in some of the highly affected states (such as Idaho) is not sufficient for capturing the
251 smoke. Although there are total 8 EPA stations in Idaho, only two of them have consistent
252 observations during the fire event; the other two stations have no valid observations, and the
253 remaining four stations have only 2~6 observations during the 17-day period. Limited valid data
254 along with unevenly distributed stations makes it hard to quantify smoke pollution in Northwestern
255 US during the fire event period. Therefore, we utilize satellite data to enlarge the spatial coverage
256 and estimate pollution at a finer spatial resolution.

257 The spatial distribution of AOD shown in Figure 2b indicates that the smoke from Canada
258 is concentrated mostly in Northern US states such as WA, Oregon, Idaho, Montana, North Dakota
259 and Minnesota. The black arrow shows the mean 800hPa-level mean wind for 17 days, and the
260 length of the arrow represents the wind speed in ms^{-1} . Also shown in Figure 2b are wind speeds
261 close to the fire sources which are about $4\sim 5 \text{ ms}^{-1}$, and according to the distances and wind
262 directions, it can take approximately 28~36 hours for the smoke to transport southeastward to
263 Washington state. Then the smoke continues to move east to other northern states such as Montana
264 and North Dakota. In addition, the grey circle represents the total fire radiative power (FRP) of
265 every 2.3×3.5 -degree box. The reason for not choosing a smaller grid for the FRP is to not clutter
266 Figure 2b with information from small fires. The bigger the circle is, the stronger the fire is in that
267 grid and different sizes and its corresponding FRP values are shown in the lower right corner. It is
268 clear that the strongest fires in 2018 are located in the Tweedsmuir Provincial Park of British

269 Columbia in Canada (53.333N, 126.417W). The four separate lightning-caused wildfires burnt
270 nearly 301,549 hectares of the boreal forest. The total FRP of August 2018 in Canada is about
271 5362 (*1000 MW), while the total FRP of August 2011 in Canada is 48 (* 1000 MW). The 2011
272 fire was relatively weak compared to the 2018 Tweedsmuir Complex fire and we therefore use the
273 2011 air quality data as a baseline to quantify the 2018 fire influence on PM_{2.5} in the United States.

274 **4.2 Model Fitting and validation**

275 The main goal for using GWR model is to help predict the spatial distribution of PM_{2.5} for
276 places with no ground monitors while leveraging the satellite AOD and therefore it is important to
277 ensure that the model is robust. Figure 3a and 3b show the results for 2018 for GWR model fitting
278 for the entire US and the LOOCV models respectively. The color of the scatter plots represents
279 the probability density function (PDF) which calculates the relative likelihood that the observed
280 ground-level PM_{2.5} would equal the predicted value. The lighter the color is, the more points are
281 present, with a higher correlation. The model fitting process estimates the slope for each variable
282 and therefore the model can be fitted close to the observed PM_{2.5} and using this estimated
283 relationship we are able to assess surface PM_{2.5} using other parameters at locations where PM_{2.5}
284 monitors are not available. The LOOCV process tests the model performance in predicting PM_{2.5}.
285 If the results of LOOCV has a large bias from the model fitting, then the predictability of the model
286 is low. Higher R² difference and RMSE difference value indicate that the model is overfitting and
287 not suitable. The R² for the model fitting is 0.834, and the R² for the LOOCV is 0.797; the RMSE
288 for the GWR model fitting is 3.46 $\mu\text{g m}^{-3}$, and for LOOCV the RMSE is 3.84 $\mu\text{g m}^{-3}$. There are
289 minor differences between fitting R² and validation R² (0.037) and between fitting RMSE and
290 validation RMSE (0.376 $\mu\text{g m}^{-3}$) suggesting that the model is not over-fitting and has stable
291 predictability further indicating that the model can predict surface PM_{2.5} reliably. In addition, we

292 also performed a 20-fold cross validation by splitting the dataset into 20 consecutive folds, and
293 each fold is used for validation while the 19 remaining folds form the training set. The 20-fold
294 cross validation has R^2 of 0.745 and RMSE of $4.3 \mu g m^{-3}$. The increase/decrease in the cross
295 validated R^2 and RMSE indicates the importance of sufficient data used for fitting since a small
296 decrease in the number of fitting data can reduce the model prediction accuracy. Overall, the
297 prediction error of the model is between $3\sim 5 \mu g m^{-3}$, which is a reasonable error range for 17-day
298 average prediction of $PM_{2.5}$. For data greater than the EPA standard ($35 \mu g m^{-3}$), the model has
299 a RMSE of $12.07 \mu g m^{-3}$, which is a lot larger than the RMSE when using the entire model.
300 Therefore, the model has a tendency for underestimating $PM_{2.5}$ exceedances by around 12.07
301 $\mu g m^{-3}$. The larger the $PM_{2.5}$ is, the greater the model underestimates. To examine the model
302 performance for high and low polluted areas, the results are divided into two parts (larger than 35
303 $\mu g m^{-3}$ and less than $35 \mu g m^{-3}$). Areas with high pollution have R^2 of 0.64 and areas with low
304 pollution have R^2 of 0.67, therefore, the model performance is relative stable for both large and
305 small $PM_{2.5}$ values. Also, the inclusion of low aerosol concentration areas does not influence the
306 model performance for high values (seen in supplemental material in figures S1 and S2), which
307 means that the high R^2 is not a reason of large number of low values.

308 **4.3 Predictors' influence during wildfires**

309 Table 4 shows the GWR model mean coefficients for the whole US region and for different
310 selected regions. The selected boxes are shown in figure 4c in different colors: box1 (red) located
311 in NW US include major fire sources in US; box2 (gold) located in Montana state is influenced
312 from both neighboring states and smoke from Canada; box3 (green) in Minnesota which is located
313 further from the fires and has minor increase in $PM_{2.5}$ due to remote smoke; box4 (black) in NE
314 (Northeast) US is the furthest from fires and has no obvious pollution increase. The second column

315 of the tables shows the conditions for sample selection and the third column shows the number of
316 pixels selected for each box. By comparing the coefficients of samples selected in these boxes,
317 predictors have different influence in different locations. AOD has stronger influence on predicting
318 $PM_{2.5}$ closer to fire sources, but local emissions become more dominant if the distances is large
319 enough. The smoke flag is overall positive related to surface $PM_{2.5}$, while it could slightly
320 negatively relate to $PM_{2.5}$ around fire sources and northeastern coasts. PBL is negatively related to
321 $PM_{2.5}$ when the pollution is concentrated near the surface (fires or human-made emissions), while
322 it appears to be positively related to $PM_{2.5}$ at locations where the main pollution source comes
323 from remote wildfire smoke. Surface temperature have a relative stable positive correlation with
324 surface $PM_{2.5}$, however, surface pressure and wind speeds are negatively correlated with $PM_{2.5}$.
325 Relative humidity, on the other hand, shows large variations on $PM_{2.5}$ influence across the nation.
326 Around the wildfires where the RH is relative low, RH has a positive correlation with $PM_{2.5}$ since
327 hygroscopicity would increase and leads to accumulation of $PM_{2.5}$, but increasing RH can also
328 decrease $PM_{2.5}$ concentration by overgrowing the $PM_{2.5}$ particles to deposition at high RH
329 environment (Chen et al., 2018).

330 From table 4, we know that the weighting for AOD is much larger than other predictors, but
331 predictors other than AOD are important for the prediction. We tested our model with AOD as the only
332 predictor to conduct a comparison with the original model, and the R^2 decreases from 0.83 to 0.79 and
333 RMSE increases from 3.46 to 3.8. This is consistent with previous study (Jiang et al., 2017) which
334 shows improvements of R^2 from 0.69 to 0.78 and RMSE from 7.25 to 6.18 by adding 4 meteorological
335 parameters in summer in easter China. Other predictors have higher weighting at the fire source region
336 (box1) where BLH cannot provide the aerosol vertical distribution information since smoke tends to
337 be injected to higher levels. For high AOD regions where aerosol tends to be suspended at high levels,
338 adding other predictors other than AOD tends to have lower improvement of the model compared with

339 low AOD values, because adding BLH can significantly improve the prediction for low level aerosols.
340 For regions with AOD less than 35, R^2 increases 0.09 from AOD only model (0.6 to 0.69), while R^2
341 increases 0.05 for areas with AOD larger than 35. RMSE decreases 12% and 7% for AOD less and
342 larger than 35 conditions, respectively. Overall, the meteorological factors have larger improvements
343 for low polluted areas (low level aerosol in this case).

344 **4.4 Predicted PM_{2.5} Distribution**

345 The mean PM_{2.5} distributions over the United States shown in Figure 4a is calculated by
346 averaging the surface PM_{2.5} data from ground monitors for the 17 days, which matches well with
347 the GWR model-predicted PM_{2.5} distributions shown in Figure 4b. The model estimation extends
348 the ground measurements and provide pollution assessments across the entire nation. Comparing
349 the AOD map (Figure 2b) with the PM_{2.5} estimations (Figure 4b), demonstrates the differences
350 between columnar and surface-level pollution. Differences between the AOD and PM_{2.5}
351 distributions are due to various reasons including 1) Areas with high PM_{2.5} concentrations in figure
352 4b correspond to low AOD values in figure 2b (Southern California, Utah, and southern US); 2)
353 and high AOD regions in figure 2b correspond to low PM_{2.5} concentrations in figure 4b
354 (Minnesota). The first situation usually occurs at the edge of polluted areas that are relative far
355 from the fire source, which is consistent with previous studies that reported smaller particles (<10
356 μg) are able to travel longer distances compared to large particles ($>10 \mu g$) (Gillies et al., 1996),
357 and that larger particles tend to settle closer to their source (Sapkota et al., 2005; Zhu et al., 2002).

358 We use the same method for August 9th to August 25th in 2011 that had low fire activity,
359 ensuring consistency for estimating coefficients for different variables for 2011. Figure 4c shows
360 the difference in spatial distribution of mean ground PM_{2.5} of the 17 days between 2018 and 2011.
361 High values of PM_{2.5} differences are in the Northwestern and central parts of the United States

362 with the Southern states having very little impact due to the fires. Of all the 48 states within the
363 study region, there are 29 states that have a higher PM_{2.5} value in 2018 than 2011, and 15 states
364 have 2018 PM_{2.5} value more than two times their 2011 value (shown in figure 5). The mean PM_{2.5}
365 for WA increases from 5.87 in 2011 to 46.47 $\mu\text{g m}^{-3}$ in 2018, which is about 8 times more than
366 2011 values. The PM_{2.5} values in Oregon increases from 4.97 (in 2011) to 33.3 $\mu\text{g m}^{-3}$ in 2018,
367 which is nearly seven times more than in 2011. For states from Montana to Minnesota, the mean
368 PM_{2.5} decreases from east to west, which reveals the path of smoke transport. As shown in Figure
369 4c, there is a clear transport path of smoke from North Dakota all the way to Texas. Along the
370 path, smoke increases PM_{2.5} concentrations by 168% in North Dakota and 27% in Texas. Smoke
371 aerosols transported over long distances contains fine fraction PM which significantly affect the
372 health of children, adults, and vulnerable groups.

373 Figure 5 shows the mean PM_{2.5} predicted from the GWR model of different EPA regions
374 for the 17 days in 2011 and 2018 (Hawaii and Alaska are not included). The most influenced region
375 is region 10, which has a 2018 mean PM_{2.5} value of 34.2 $\mu\text{g m}^{-3}$ that is 6 times larger than the
376 values in 2011 (5.8 $\mu\text{g m}^{-3}$) values. The PM_{2.5} of region 8 and 9 have 2.4 and 2.6 times increase
377 in 2018 compared to 2011. Region 1~4 have lower PM_{2.5} in 2018 than 2011 possibly due to Clean
378 Air Act initiatives, absence of any major fire activities and further away for transported aerosols.
379 The emission reduction improves the US air quality and lower the PM_{2.5} every year, but 6 out of
380 10 EPA regions show significant increases in PM_{2.5} during the study period, which indicates that
381 the long-range transported wildfire smoke has become the new major pollutant in the US.

382 **4.5 Estimation of Canadian fire pollution**

383 To evaluate the pollution caused only from Canadian fires, we did a rough assessment
384 according to the total FRP and PM_{2.5} values. There are three states in the US have wildfires during

385 the study period: California, Washington and Oregon, and they have total FRP of 1186, 518 and
386 439 (*1000 MW) respectively. Assuming that California was only influenced by the local fires,
387 then fires of 1186 (*1000 MW) cause $13 \mu\text{g m}^{-3}$ increase in $\text{PM}_{2.5}$. Accordingly, wildfires in
388 Washington and Oregon State will cause 6 and $5 \mu\text{g m}^{-3}$ increase in state mean $\text{PM}_{2.5}$. Therefore,
389 Canadian fires caused $\text{PM}_{2.5}$ increase in Washington and Oregon is about 35 and $23 \mu\text{g m}^{-3}$. Since
390 the FRP of Canadian wildfires are approximately 5 times larger than that of the California fires,
391 which is the strongest fire in US, we assume the pollution affecting the states located in the
392 downwind directions other than the three states are mainly coming from Canadian wildfires. States
393 with no local fires such as Montana, North Dakota, South Dakota and Minnesota have $\text{PM}_{2.5}$
394 increase of 18.31, 12.8, 10.4 and $10.13 \mu\text{g m}^{-3}$. The decrease of these numbers reveal that the
395 smoke is transport in a SE direction. This influence of Canadian wildfires on US air quality is only
396 a rough quantity estimation, thus additional work is needed for understand long-range transport
397 smoke pollution and its impact on public health. One way to do this would be assessing the
398 difference of pollution by turning on and off US fires in chemistry models.

399 **4.6 Comparison with previous studies**

400 Comparing with the Bayesian ensemble model developed by Geng et al. (Geng et al., 2018)
401 using MAIAC AOD and CMAQ (Community Multiscale Air Quality) model and ground $\text{PM}_{2.5}$
402 measurements, our GWR model has larger R^2 , but with the chemistry transport model (CTM),
403 their method can provide more vertical distribution information which is important for wildfire
404 smoke. GWR usually have better accuracy than CTM since there are large uncertainties related to
405 different CTM inputs such as emission, meteorological and land cover data, but for regions with
406 less or no ground measurements, CTM provide a great approach for estimating surface $\text{PM}_{2.5}$.
407 Other studies which used machine learning method to predict surface $\text{PM}_{2.5}$ have better

408 performance for long-term prediction rather than monthly estimation (Liang et al., 2020; Xiao et
409 al., 2018), but can better resolve complex relationship between different predictors than statistical
410 models (Geng et al., 2020). For wildfire events, the available data is much less than the long-term
411 aerosol analysis, so the performance of machine learning method could be less accurate compared
412 to long-term prediction. Our study also shows slightly larger R^2 compared to other GWR studies
413 (Hu et al., 2013; Ma et al., 2014; You et al., 2016) due to the inclusion of more meteorological and
414 other related predictors.

415 **4.7 Model uncertainties and limitations**

416 There are various sources of uncertainties and limitations for studies that use satellite data
417 to estimate surface $PM_{2.5}$ concentrations. Since wildfires develop quickly it is important to have
418 continuous observations to capture the rapid changes. This study uses polar orbiting high-quality
419 satellite aerosol products, but the temporal evolution can only be estimated by geostationary data
420 sets. Although satellite observations have excellent spatial coverage, missing data due to cloud
421 cover is a limitation. As discussed in the paper, the prediction error (RMSE) of the model is
422 between $3\sim 5 \mu g m^{-3}$, while the RMSE increased for locations with high aerosol concentration.
423 This is partly due to lack of accurate vertical distribution information which is very important for
424 wildfire smoke. The GWR model is largely influenced by the distribution of ground stations, and
425 the prediction error will be different in different places due to unevenly distributed $PM_{2.5}$ stations.
426 For locations that have a dense ground-monitoring distribution, the prediction error will be low,
427 while the prediction error will be relative larger at other places with sparse surface stations.
428 Although there are obvious limitations, complementing surface data with satellite products and
429 meteorological and other ancillary information in a statistical model like the GWR has provided
430 robust results for estimating surface $PM_{2.5}$ from wildfires. We also note that we did not consider

431 some variables used in other studies such as NDVI, forest cover, vegetation type, industrial
432 density, visibility and chemical constituents of smoke particles (Donkelaar et al., 2015; Hu et al.,
433 2013; You et al., 2015; Zou et al., 2016). Visibility mentioned in some studies may improve the
434 model performance, but unlike AOD, it has limited measurement across the nation, which will
435 restrict the applicability of training data. Another uncertainty comes from the 2011 wildfires which
436 we assumed to be zero fire events but there are actually few fire events in EPA region 6, 8, 9 and
437 10, and this will lead to underestimation of $PM_{2.5}$ increase due to 2018 fires in these regions.

438 One limitation of this study is that analysis based on 17-day mean values cannot capture
439 daily pollution variations, which is also very important for pollution estimation during rapid-
440 changing wildfire events. To extend this analysis to daily estimation, the cloud contaminations of
441 satellite observations become a major problem. Therefore, future work is needed using chemistry
442 transport models and other data to fill in the gaps on missing AOD data due to cloud coverage.

443 **5. Summary and Conclusions**

444 We estimate the surface mean $PM_{2.5}$ for 17 days in August for a high fire active year (2018)
445 and compare that with a low fire activity year using the Geographically Weighted Regression
446 (GWR) method to assess the increase in $PM_{2.5}$ in the United States due to smoke transported from
447 fires. The difference in $PM_{2.5}$ between the two years indicates that more than half of the US states
448 (29 states) are influenced by the NWUSC wildfires, and half of the affected states have 17-day
449 mean $PM_{2.5}$ increases larger than 100% of the baseline value. The peak $PM_{2.5}$ during the wildfires
450 can be much larger than the 17-day average and can affect vulnerable populations susceptible to
451 air pollution. Some of the most affected states are in Washington, California, Wisconsin, Colorado
452 and Oregon, all of which have populations greater than 4 million. According to CDC (Centers for
453 Disease Control and Prevention), 8% of the population have asthma (CDC, 2011). Therefore, for

454 asthma alone, there are about 3 million people facing significant health issue due to the long-range
455 transport smoke in these states.

456 For states that show decrease in PM_{2.5} due to the Clean Air Act, the mean decrease is about
457 16% of the baseline after 7 years. This is consistent with EPA's report that there is a 23% decrease
458 of PM_{2.5} in national average from 2010 to 2019(U.S. Environmental Protection Agency, 2019).
459 Comparing with the dramatic increase (132%) caused by wildfires, pollution from the fires is
460 counteracting our effort on emission controls. Although wildfires are often episodic and short-
461 term, high frequency of fire occurrence and increasing longer durations of summertime wildfires
462 in recent years has made them now a long-term influence on public lives. Our results show a
463 significant increase of pollution in a short time period in most of the US states due to the NWUSC
464 wildfires, which affects millions of people. With wildfires becoming more frequent during recent
465 years, more effort is needed to predict and warn the public about the long-range transported smoke
466 from wildfires.

467 **Acknowledgements.**

468 Pawan Gupta was supported by a NASA Grant. MODIS data were acquired from the Goddard
469 DAAC. Sincerest thanks to the MAIAC, MODIS, EPA and ECMWF teams for their datasets that
470 makes this research possible.

471 **References**

472 Apte, J.S., Brauer, M., Cohen, A.J., Ezzati, M., Pope, C.A., 2018. Ambient PM_{2.5} Reduces
473 Global and Regional Life Expectancy. *Environ. Sci. Technol. Lett.* 5, 546–551.
474 <https://doi.org/10.1021/acs.estlett.8b00360>

475 Brunsdon, C., Fotheringham, A.S., Charlton, M.E., 1996. Geographically Weighted Regression:

- 476 A Method for Exploring Spatial Nonstationarity. *Geogr. Anal.* 28, 281–298.
477 <https://doi.org/https://doi.org/10.1111/j.1538-4632.1996.tb00936.x>
- 478 Calkin, D.E., Thompson, M.P., Finney, M.A., 2015. Negative consequences of positive
479 feedbacks in us wildfire management. *For. Ecosyst.* 2, 1–10.
480 <https://doi.org/10.1186/s40663-015-0033-8>
- 481 Cascio, W.E., 2018. Wildland Fire Smoke and Human Health. *Sci. Total Environ.* 624, 586–595.
482 <https://doi.org/10.1016/j.scitotenv.2017.12.086>.
- 483 CDC, 2011. Asthma in the US. *CDC Vital Signs* 1–4.
- 484 Chen, D., Xie, X., Zhou, Y., Lang, J., Xu, T., Yang, N., Zhao, Y., Liu, X., 2017. Performance
485 evaluation of the WRF-chem model with different physical parameterization schemes
486 during an extremely high PM_{2.5} pollution episode in Beijing. *Aerosol Air Qual. Res.* 17,
487 262–277. <https://doi.org/10.4209/aaqr.2015.10.0610>
- 488 Chen, Z., Chen, D., Zhao, C., Kwan, M. po, Cai, J., Zhuang, Y., Zhao, B., Wang, X., Chen, B.,
489 Yang, J., Li, R., He, B., Gao, B., Wang, K., Xu, B., 2020. Influence of meteorological
490 conditions on PM_{2.5} concentrations across China: A review of methodology and
491 mechanism. *Environ. Int.* 139, 105558. <https://doi.org/10.1016/j.envint.2020.105558>
- 492 Chen, Z., Xie, X., Cai, J., Chen, D., Gao, B., He, B., Cheng, N., Xu, B., 2018. Understanding
493 meteorological influences on PM_{2.5} concentrations across China: A temporal and spatial
494 perspective. *Atmos. Chem. Phys.* 18, 5343–5358. <https://doi.org/10.5194/acp-18-5343-2018>
- 495 Chu, Y., Liu, Y., Li, X., Liu, Z., Lu, H., Lu, Y., Mao, Z., Chen, X., Li, N., Ren, M., Liu, F., Tian,
496 L., Zhu, Z., Xiang, H., 2016. A review on predicting ground PM_{2.5} concentration using

- 497 satellite aerosol optical depth. *Atmosphere (Basel)*. 7, 129.
498 <https://doi.org/10.3390/atmos7100129>
- 499 Coogan, S.C.P., Robinne, F.N., Jain, P., Flannigan, M.D., 2019. Scientists' warning on wildfire
500 — a canadian perspective. *Can. J. For. Res.* 49, 1015–1023. [https://doi.org/10.1139/cjfr-](https://doi.org/10.1139/cjfr-2019-0094)
501 2019-0094
- 502 Donkelaar, A. Van, Martin, R. V., Li, C., Burnett, R.T., 2019. Regional Estimates of Chemical
503 Composition of Fine Particulate Matter Using a Combined Geoscience-Statistical Method
504 with Information from Satellites, Models, and Monitors. *Environ. Sci. Technol.* 53, 2595–
505 2611. <https://doi.org/10.1021/acs.est.8b06392>
- 506 Donkelaar, A. Van, Martin, R. V., Park, R.J., 2006. Estimating ground-level PM_{2.5} using
507 aerosol optical depth determined from satellite remote sensing. *J. Geophys. Res. Atmos.*
508 111. <https://doi.org/10.1029/2005JD006996>
- 509 Donkelaar, A. Van, Martin, R. V., Spurr, R.J.D., Burnett, R.T., 2015. High-Resolution Satellite-
510 Derived PM_{2.5} from Optimal Estimation and Geographically Weighted Regression over
511 North America. *Environ. Sci. Technol.* 49, 10482–10491.
512 <https://doi.org/10.1021/acs.est.5b02076>
- 513 Dreessen, J., Sullivan, J., Delgado, R., 2016. Observations and impacts of transported Canadian
514 wildfire smoke on ozone and aerosol air quality in the Maryland region on June 9–12, 2015.
515 *J. Air Waste Manag. Assoc.* 66, 842–862. <https://doi.org/10.1080/10962247.2016.1161674>
- 516 Fotheringham, A.S., Charlton, M.E., Brunson, C., 1998. Geographically weighted regression: a
517 natural evolution of the expansion method for spatial data analysis. *Environ. Plan. A* 30,
518 1905–1927.

- 519 Fotheringham, S.A., Brunsdon, C., Charlton, M., 2003. Geographically Weighted Regression :
520 The Analysis of Spatially Varying Relationships, John Wiley and Sons.
- 521 Freeborn, P.H., Wooster, M.J., Roy, D.P., Cochrane, M.A., 2014. Quantification of MODIS fire
522 radiative power (FRP) measurement uncertainty for use in satellite-based active fire
523 characterization and biomass burning estimation. *Geophys. Res. Lett.* 41, 1988–1994.
524 <https://doi.org/10.1002/2013GL059086>.
- 525 Goldberg, D.L., Gupta, P., Wang, K., Jena, C., Zhang, Y., Lu, Z., Streets, D.G., 2019. Using gap-
526 filled MAIAC AOD and WRF-Chem to estimate daily PM_{2.5} concentrations at 1 km
527 resolution in the Eastern United States. *Atmos. Environ.* 199, 443–452.
528 <https://doi.org/10.1016/j.atmosenv.2018.11.049>
- 529 Gu, Y., 2019. Estimating PM_{2.5} Concentrations Using 3 km MODIS AOD Products : A Case
530 Study in British Columbia , Canada. University of Waterloo.
- 531 Guo, B., Wang, X., Pei, L., Su, Y., Zhang, D., Wang, Y., 2021. Identifying the spatiotemporal
532 dynamic of PM_{2.5} concentrations at multiple scales using geographically and temporally
533 weighted regression model across China during 2015–2018. *Sci. Total Environ.* 751.
534 <https://doi.org/10.1016/j.scitotenv.2020.141765>
- 535 Gupta, P., Christopher, S.A., 2009a. Particulate matter air quality assessment using integrated
536 surface, satellite, and meteorological products: 2. A neural network approach. *J. Geophys.*
537 *Res. Atmos.* 114, 1–14. <https://doi.org/10.1029/2008JD011497>
- 538 Gupta, P., Christopher, S.A., 2009b. Particulate matter air quality assessment using integrated
539 surface , satellite , and meteorological products : Multiple regression approach. *J. Geophys.*
540 *Res. Atmos.* 114, 1–13. <https://doi.org/10.1029/2008JD011496>

- 541 Haarig, M., Ansmann, A., Baars, H., Jimenez, C., Veselovskii, I., Engelmann, R., Althausen, D.,
542 2018. Extreme levels of Canadian wildfire smoke in the stratosphere over central Europe –
543 Part 2: Lidar study of depolarization and lidar ratios at 355, 532, and 1064 nm and of
544 microphysical properties. *Atmos. Chem. Phys. Discuss.* 1–22. [https://doi.org/10.5194/acp-](https://doi.org/10.5194/acp-2018-358)
545 2018-358
- 546 Hall, E.S., Kaushik, S.M., Vanderpool, R.W., Duvall, R.M., Beaver, M.R., Long, R.W.,
547 Solomon, P.A., 2013. Intergrating Sensor Monitoring Technology into Current Air
548 Pollution Regulatory Support Paradigm: Practical Considerations. *Am. J. Environ. Eng* 4,
549 147–154. <https://doi.org/10.5923/j.ajee.20140406.02>
- 550 Hessburg, P.F., Churchill, D.J., Larson, A.J., Haugo, R.D., Miller, C., Spies, T.A., North, M.P.,
551 Povak, N.A., Belote, R.T., Singleton, P.H., Gaines, W.L., Keane, R.E., Aplet, G.H.,
552 Stephens, S.L., Morgan, P., Bisson, P.A., Rieman, B.E., Salter, R.B., Reeves, G.H., 2015.
553 Restoring fire-prone Inland Pacific landscapes: seven core principles. *Landsc. Ecol.* 30,
554 1805–1835. <https://doi.org/10.1007/s10980-015-0218-0>
- 555 Hoff, R.M., Christopher, S.A., 2009. Remote Sensing of Particulate Pollution from Space : Have
556 We Reached the Promised Land ? *J. Air Waste Manage. Assoc.* 59, 645–675.
557 <https://doi.org/10.3155/1047-3289.59.6.645>
- 558 Hu, X., Waller, L.A., Al-Hamdan, M.Z., Crosson, W.L., Estes, M.G., Estes, S.M., Quattrochi,
559 D.A., Sarnat, J.A., Liu, Y., 2013. Estimating ground-level PM_{2.5} concentrations in the
560 southeastern U.S. using geographically weighted regression. *Environ. Res.* 121, 1–10.
561 <https://doi.org/10.1016/j.envres.2012.11.003>
- 562 Hu, Z., 2009. Spatial analysis of MODIS aerosol optical depth, PM_{2.5}, and chronic coronary

- 563 heart disease. *Int. J. Health Geogr.* 8, 1–10. <https://doi.org/10.1186/1476-072X-8-27>
- 564 Hubbell, B.J., Crume, R. V., Evarts, D.M., Cohen, J.M., 2010. Policy Monitor: Regulation and
565 progress under the 1990 Clean Air Act Amendments. *Rev. Environ. Econ. Policy* 4, 122–
566 138. <https://doi.org/10.1093/reep/rep019>
- 567 Hystad, P., Demers, P.A., Johnson, K.C., Brook, J., Van Donkelaar, A., Lamsal, L., Martin, R.,
568 Brauer, M., 2012. Spatiotemporal air pollution exposure assessment for a Canadian
569 population-based lung cancer case-control study. *Environ. Heal. A Glob. Access Sci.*
570 *Source* 11, 1–22. <https://doi.org/10.1186/1476-069X-11-22>
- 571 J.A.Gillies, W.G.Nickling, G.H.Mctainsh, 1996. Dust concentration s and particle-size
572 characteristics of an intense dust haze event: inland delta region. *Atmos. Environ.* 30, 1081–
573 1090.
- 574 Kearns, M., Ron, D., 1999. Algorithmic stability and sanity-check bounds for leave-one-out
575 cross-validation. *Neural Comput.* 11, 1427–1453.
576 <https://doi.org/10.1162/089976699300016304>
- 577 Koelemeijer, R.B.A., Homan, C.D., Matthijsen, J., 2006. Comparison of spatial and temporal
578 variations of aerosol optical thickness and particulate matter over Europe. *Atmos. Environ.*
579 40, 5304–5315. <https://doi.org/10.1016/j.atmosenv.2006.04.044>
- 580 Kollanus, V., Tiittanen, P., Niemi, J. V., Lanki, T., 2016. Effects of long-range transported air
581 pollution from vegetation fires on daily mortality and hospital admissions in the Helsinki
582 metropolitan area, Finland. *Environ. Res.* 151, 351–358.
583 <https://doi.org/10.1016/j.envres.2016.08.003>

- 584 Liu, Y., Sarnat, J.A., Kilaru, V., Jacob, D.J., Koutrakis, P., 2005. Estimating ground-level PM_{2.5}
585 in the eastern United States using satellite remote sensing. *Environ. Sci. Technol.* 39, 3269–
586 3278. <https://doi.org/10.1021/es049352m>
- 587 Loader, C.R., 1999. BANDWIDTH SELECTION: CLASSICAL OR PLUG-IN? *Ann. Stat.* 27,
588 415–438.
- 589 Lyapustin, A., Korkin, S., Wang, Y., Quayle, B., Laszlo, I., 2012. Discrimination of biomass
590 burning smoke and clouds in MAIAC algorithm. *Atmos. Chem. Phys.* 12, 9679–9686.
591 <https://doi.org/10.5194/acp-12-9679-2012>
- 592 Lyapustin, A., Wang, Y., Korkin, S., Huang, D., 2018. MODIS Collection 6 MAIAC Algorithm.
593 *Atmos. Meas. Tech.* 11, 5741–5765. <https://doi.org/10.5194/amt-2018-141>
- 594 Ma, Z., Hu, X., Huang, L., Bi, J., Liu, Y., 2014. Estimating ground-level PM_{2.5} in china using
595 satellite remote sensing. *Environ. Sci. Technol.* 48, 7436–7444.
596 <https://doi.org/10.1021/es5009399>
- 597 Meixner, T., Wohlgemuth, P., 2004. Wildfire Impacts on Water Quality. *J. Wildl. Fire* 13, 27–
598 35.
- 599 Melillo, J.M., Richmond, T., Yohe, G.W., 2014. Climate Change Impacts in the United States.
600 *Third Natl. Clim. Assess.* 52. <https://doi.org/10.7930/J0Z31WJ2>.
- 601 Miao, Y., Liu, S., Guo, J., Huang, S., Yan, Y., Lou, M., 2018. Unraveling the relationships
602 between boundary layer height and PM_{2.5} pollution in China based on four-year radiosonde
603 measurements. *Environ. Pollut.* 243, 1186–1195.
604 <https://doi.org/10.1016/j.envpol.2018.09.070>

- 605 Miller, D.J., Sun, K., Zondlo, M.A., Kanter, D., Dubovik, O., Welton, E.J., Winker, D.M.,
606 Ginoux, P., 2011. Assessing boreal forest fire smoke aerosol impacts on U.S. air quality: A
607 case study using multiple data sets. *J. Geophys. Res. Atmos.* 116.
608 <https://doi.org/10.1029/2011JD016170>
- 609 Mirzaei, M., Bertazzon, S., Couloigner, I., 2018. Modeling Wildfire Smoke Pollution by
610 Integrating Land Use Regression and Remote Sensing Data : Regional Multi-Temporal
611 Estimates for Public Health and Exposure Models. *Atmosphere (Basel)*. 9, 335.
612 <https://doi.org/10.3390/atmos9090335>
- 613 Munoz-alpizar, R., Pavlovic, R., Moran, M.D., Chen, J., Gravel, S., Henderson, S.B., Sylvain,
614 M., Racine, J., Duhamel, A., Gilbert, S., Beaulieu, P., Landry, H., Davignon, D., Cousineau,
615 S., Bouchet, V., 2017. Multi-Year (2013–2016) PM_{2.5} Wildfire Pollution Exposure over
616 North America as Determined from Operational Air Quality Forecasts. *Atmosphere (Basel)*.
617 8, 179. <https://doi.org/10.3390/atmos8090179>
- 618 Navarro, K.M., Schweizer, D., Balmes, J.R., Cisneros, R., 2018. A review of community smoke
619 exposure from wildfire compared to prescribed fire in the United States. *Atmosphere*
620 *(Basel)*. 9, 1–11. <https://doi.org/10.3390/atmos9050185>
- 621 Samet, J.M., 2011. The clean air act and health - A clearer view from 2011. *N. Engl. J. Med.*
622 365, 198–201. <https://doi.org/10.1056/NEJMp1103332>
- 623 Sapkota, A., Symons, J.M., Kleissl, J., Wang, L., Parlange, M.B., Ondov, J., Breyse, P.N.,
624 Diette, G.B., Eggleston, P.A., Buckley, T.J., 2005. Impact of the 2002 Canadian forest fires
625 on particulate matter air quality in Baltimore City. *Environ. Sci. Technol.* 39, 24–32.
626 <https://doi.org/10.1021/es035311z>

- 627 Stephens, S.L., 2005. Forest fire causes and extent on United States Forest Service lands. *Int. J.*
628 *Wildl. Fire* 14, 213–222. <https://doi.org/10.1071/WF04006>
- 629 Trueblood, M.B., Lobo, P., Hagen, D.E., Achterberg, S.C., Liu, W., Whitefield, P.D., 2018.
630 Application of a hygroscopicity tandem differential mobility analyzer for characterizing PM
631 emissions in exhaust plumes from an aircraft engine burning conventional and alternative
632 fuels. *Atmos. Chem. Phys.* 18, 17029–17045. <https://doi.org/10.5194/acp-18-17029-2018>
- 633 U.S. Environmental Protection Agency, 2019. Particulate Matter (PM_{2.5}) Trends.
- 634 Wang, H., Shi, G., Tian, M., Zhang, L., Chen, Y., Yang, F., Cao, X., 2017. Aerosol optical
635 properties and chemical composition apportionment in Sichuan Basin, China. *Sci. Total*
636 *Environ.* 577, 245–257. <https://doi.org/10.1016/j.scitotenv.2016.10.173>
- 637 Xu, T., Song, Y., Liu, M., Cai, X., Zhang, H., Guo, J., Zhu, T., 2019. Temperature inversions in
638 severe polluted days derived from radiosonde data in North China from 2011 to 2016. *Sci.*
639 *Total Environ.* 647, 1011–1020. <https://doi.org/10.1016/j.scitotenv.2018.08.088>
- 640 You, T., Wu, R., Huang, G., Fan, G., 2017. Regional meteorological patterns for heavy pollution
641 events in Beijing. *J. Meteorol. Res.* 31, 597–611. [https://doi.org/10.1007/s13351-017-6143-](https://doi.org/10.1007/s13351-017-6143-1)
642 1
- 643 You, W., Zang, Z., Pan, X., Zhang, L., Chen, D., 2015. Estimating PM_{2.5} in Xi'an, China using
644 aerosol optical depth: A comparison between the MODIS and MISR retrieval models. *Sci.*
645 *Total Environ.* 505, 1156–1165. <https://doi.org/10.1016/j.scitotenv.2014.11.024>
- 646 You, W., Zang, Z., Zhang, L., Li, Y., Pan, X., Wang, W., 2016. National-scale estimates of
647 ground-level PM_{2.5} concentration in China using geographically weighted regression based

648 on 3 km resolution MODIS AOD. *Remote Sens.* 8. <https://doi.org/10.3390/rs8030184>

649 Zhang, H., Hoff, R.M., Engel-Cox, J.A., 2009. The relation between moderate resolution
650 imaging spectroradiometer (MODIS) aerosol optical depth and PM_{2.5} over the United
651 States: A geographical comparison by U.S. Environmental Protection Agency regions. *J.*
652 *Air Waste Manag. Assoc.* 59, 1358–1369. <https://doi.org/10.3155/1047-3289.59.11.1358>

653 Zhang, H., Wang, Y., Hu, J., Ying, Q., Hu, X.M., 2015. Relationships between meteorological
654 parameters and criteria air pollutants in three megacities in China. *Environ. Res.* 140, 242–
655 254. <https://doi.org/10.1016/j.envres.2015.04.004>

656 Zheng, C., Zhao, C., Zhu, Y., Wang, Y., Shi, X., Wu, X., Chen, T., Wu, F., Qiu, Y., 2017.
657 Analysis of influential factors for the relationship between PM_{2.5} and AOD in Beijing.
658 *Atmos. Chem. Phys.* 17, 13473–13489. <https://doi.org/10.5194/acp-17-13473-2017>

659 Zhu, Y., Hinds, W.C., Kim, S., Sioutas, C., 2002. Concentration and size distribution of ultrafine
660 particles near a major highway. *J. Air Waste Manag. Assoc.* 52, 1032–1042.
661 <https://doi.org/10.1080/10473289.2002.10470842>

662 Zou, B., Pu, Q., Bilal, M., Weng, Q., Zhai, L., Nichol, J.E., 2016. High-resolution Satellite
663 Mapping of Fine Particulates Based on Geographically Weighted Regression. *Ieee Geosci.*
664 *Remote Sens. Lett.* 13, 495–499.

665

666

667 Table 1. Datasets used in the study with sources.

668

	Data /Model	Sensor	Spatial Resolution	Temporal Resolution	Accuracy
1	Surface PM _{2.5}	TEOM	Point data	daily	±5~10%
2	Mid visible aerosol optical depth (AOD)	MAIAC_ MODIS	1km	daily	66% compared to AERONET
3	Fire Radiative Power (FRP)	Terra/Aqua- MODIS	1km	daily	± 7%
4	ECMWF (Meteorological variables)		0.25 degree	hourly	

669 1) <https://www.epa.gov/outdoor-air-quality-data>

670 2) <https://earthdata.nasa.gov/>

671 3) <https://earthdata.nasa.gov/>

672 4) <https://www.ecmwf.int/en/forecasts>

673

674

675

676 Table 2. Total FRP in Canada and Northwestern US in August of Different Years (unit: 10⁴

677 MW)

Year	2010	2011	2012	2013	2014	2015	2016	2017	2018
CA	148.24	4.84	19.93	70.54	107.78	10.39	4.6	307.3	542.99
NW US	16.41	42.84	320.39	192.06	67.01	339.58	112.9	195.64	296.91

678

679 Table 3. statistics of 15 states that violate EPA standards (35 $\mu\text{g m}^{-3}$) during the 17-day wildfire
680 period

State	number of site violate standard	number of site in the state	Percentage of site violate standard (%)	number of days violate standard
Montana	14	15	93.34	16
Washington	18	20	90	16
Oregon	12	14	85.71	5
North Dakota	7	11	63.63	4
Idaho	5	8	62.5	8
Colorado	11	21	52.38	2
South Dakota	5	10	50	1
California	57	119	47.9	14
Utah	7	15	46.67	4
Nevada	4	13	30.77	1
Wyoming	7	24	29.2	2
Minnesota	4	26	15.4	2
Texas	3	37	8.1	1
Louisiana	1	14	7.1	1
Arizona	1	20	5	1

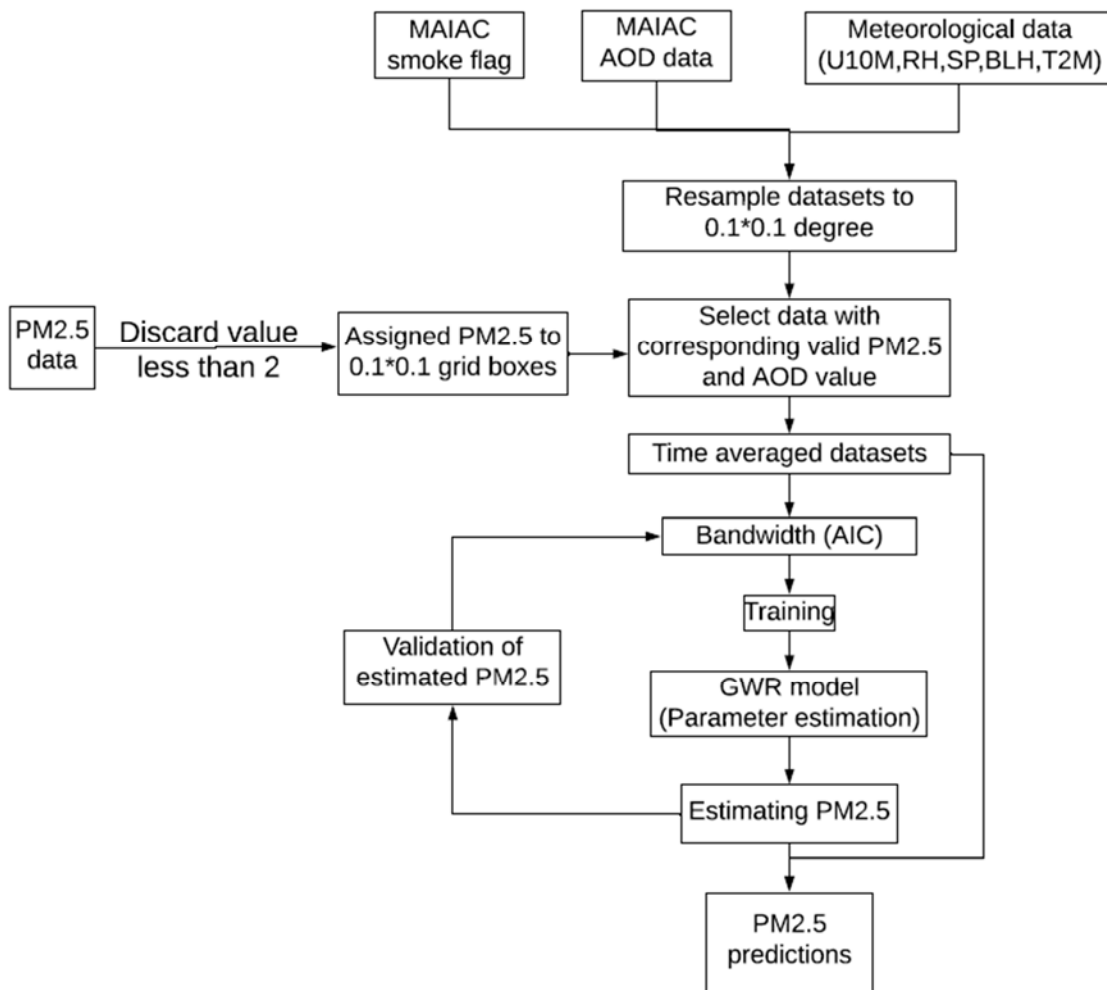
681

682 Table 4. Coefficients of different predictors

Mean coefficients	sample selection	N	AOD	smoke flag	PBL	T2M	RH	U	SP
box1(red)	FRP>1000	213	91.94	-0.14	-2.25	0.33	0.08	-2	-0.06
box2(gold)	PM2.5>30	362	60.1	0.013	-2.9	0.23	-0.08	-1.6	-0.03
box3(green)	PM2.5>17	278	6.2	0.05	0.2	0.2	0.014	-0.3	-0.02
box4(black)	17>PM2.5>10	938	7.1	-0.02	-1.2	0.22	-0.035	0.06	-0.005
whole US region	~	106352	28.1	0.024	-0.9	0.06	-0.04	-0.7	-0.002

683

684



685

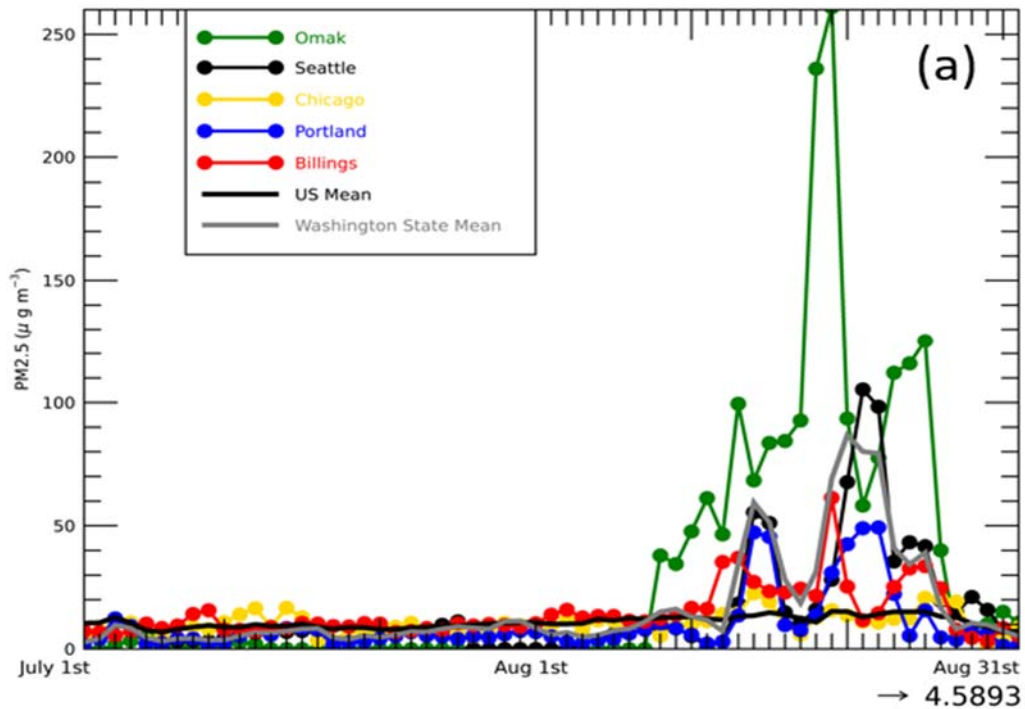
686 Figure 1. Flow chart for the Geographically Weighted Regression model used. All satellite,

687 ground, meteorological data are gridded to 0.1 by 0.1 degrees.

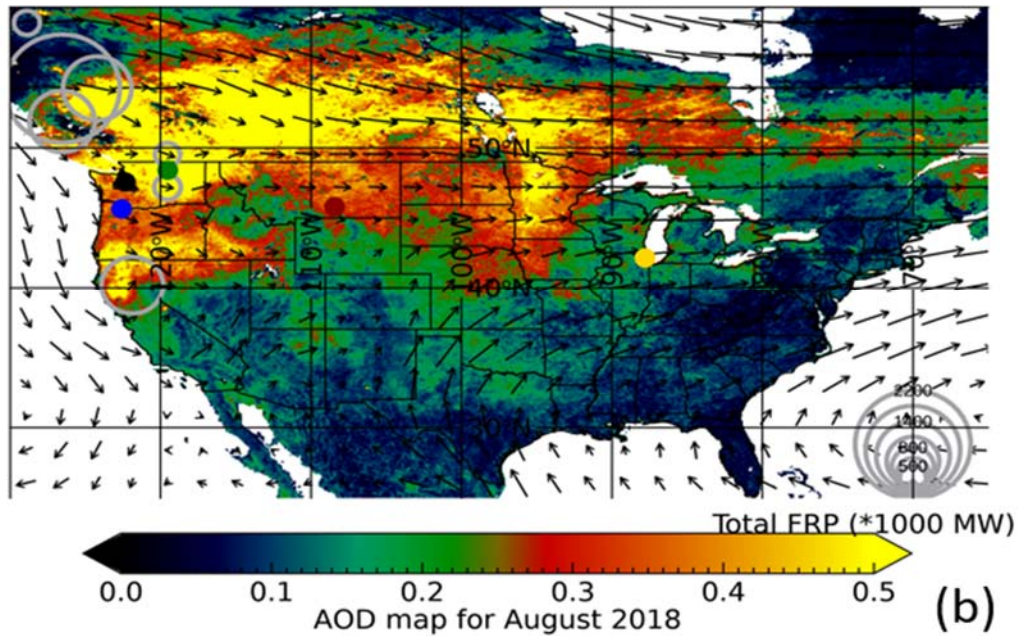
688

689

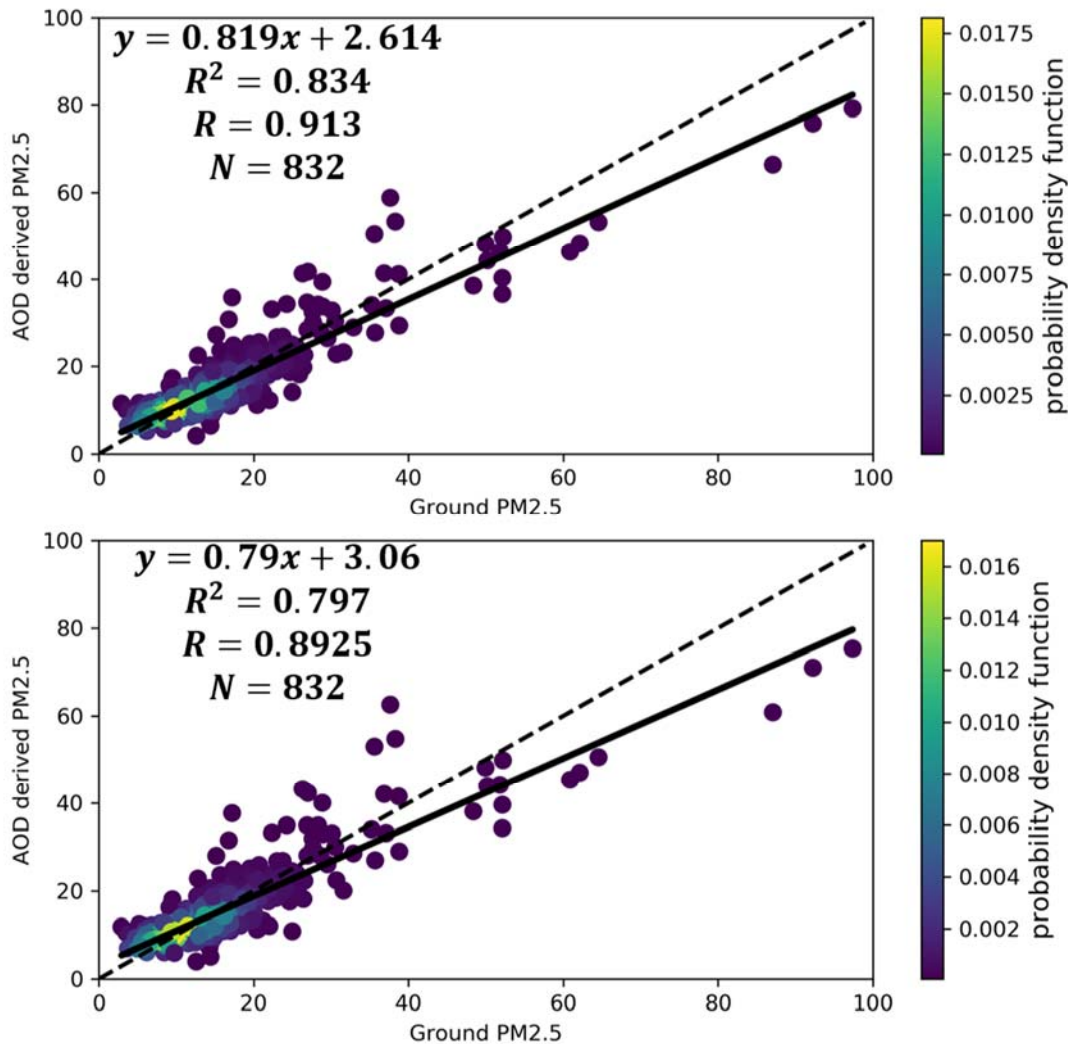
690



691



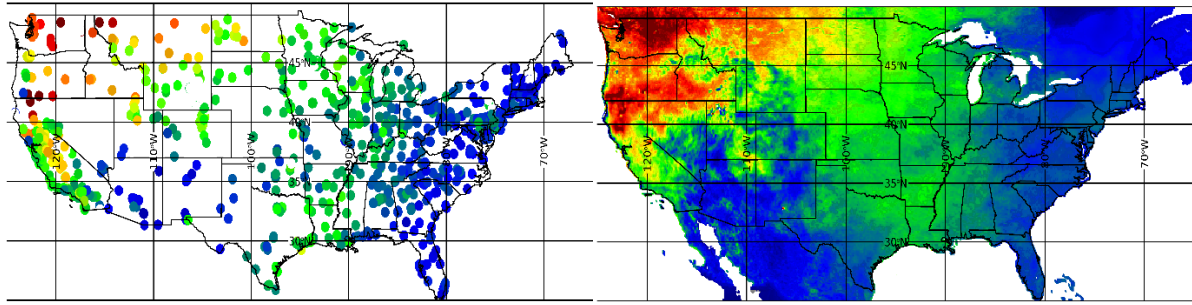
692 Figure 2. (a) Variations of EPA ground observed PM_{2.5} in different cities from July to August
 693 2018 (Omak-Washington, Seattle-Washington, Chicago-Illinois, Portland-Oregon, Billings-
 694 Montana). Black line without markers shows the mean variation of the whole US stations and the
 695 grey line without markers shows the mean variation of stations in Washington state. (b) Mean
 696 MAIAC satellite AOD distribution from August 9th to August 25th, 2018. AOD values equal or
 697 larger than 0.5 are shown as the same color (yellow). Also shown are circles with Fire Radiative
 698 Power (FRP). Black arrow shows the wind direction and the length of it represents the wind
 699 speed. The round spots of different colors on the map show the locations of the five selected
 700 cities (green-Omak, black-Seattle, yellow-Chicago, blue-Portland, red-Billings).



701
 702 Figure 3. Results of model fitting and cross validation for GWR model for the entire US region
 703 averaged from August 9th to August 25th, 2018. (a) GWR model fitting results (b) GWR model
 704 LOOCV results. The dash line is the 1:1 line as reference and the black line shows the regression
 705 line. The color of the scatter plots represents the probability density function which provides a
 706 relative likelihood that the value of the random variable would equal a certain sample.

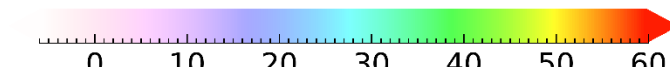
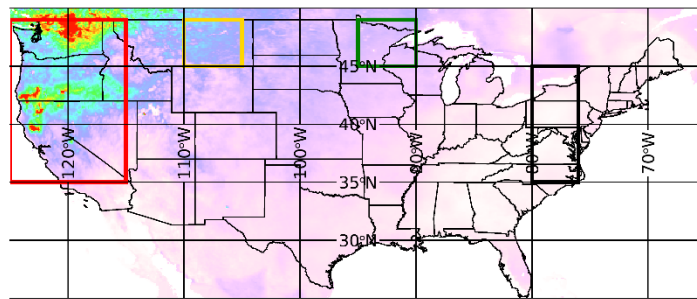
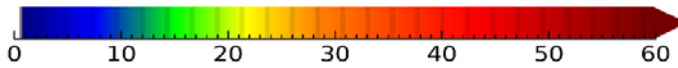
707
 708
 709
 710
 711
 712
 713

714



715

716

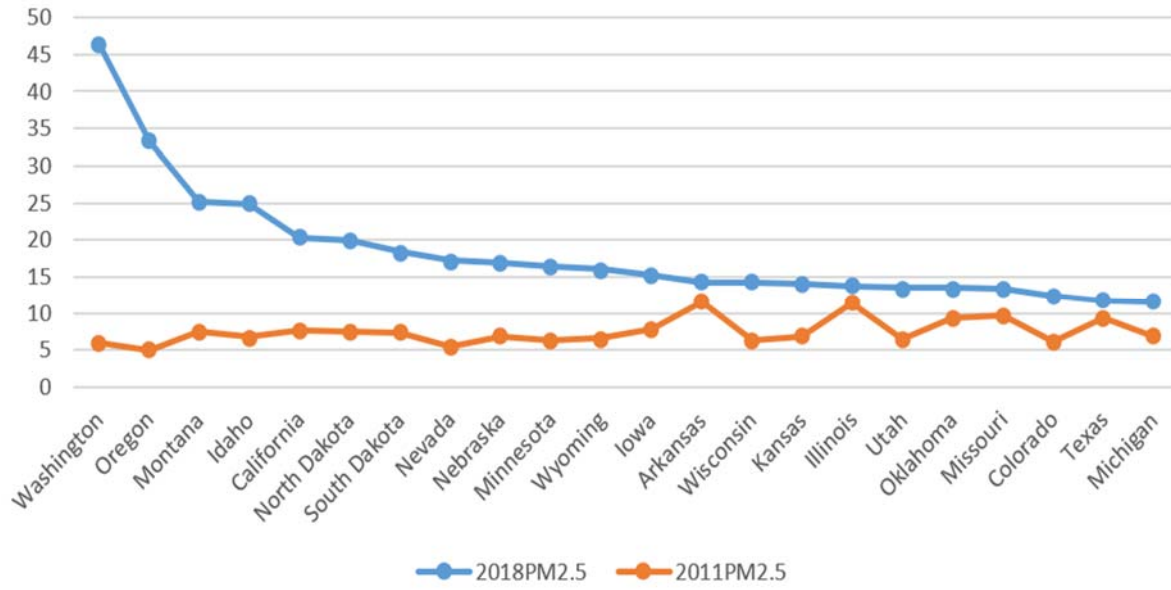


D-PM_{2.5} map between 2018 and 2011 August

717

718 Figure 4. (a) EPA ground observed PM_{2.5} distribution over the US averaged from August 9th to
 719 August 25th, 2018. (b) GWR predicted 17-day mean PM_{2.5} distribution. (c) Difference map of
 720 predicted ground PM_{2.5} of the 17-day mean values between 2018 and 2011. PM_{2.5} values equal or
 721 larger than $60 \mu\text{g m}^{-3}$ are shown as the same color (red). Note that the D-PM_{2.5} has a different
 722 color scale to make the negative values more apparent (blue).
 723

724



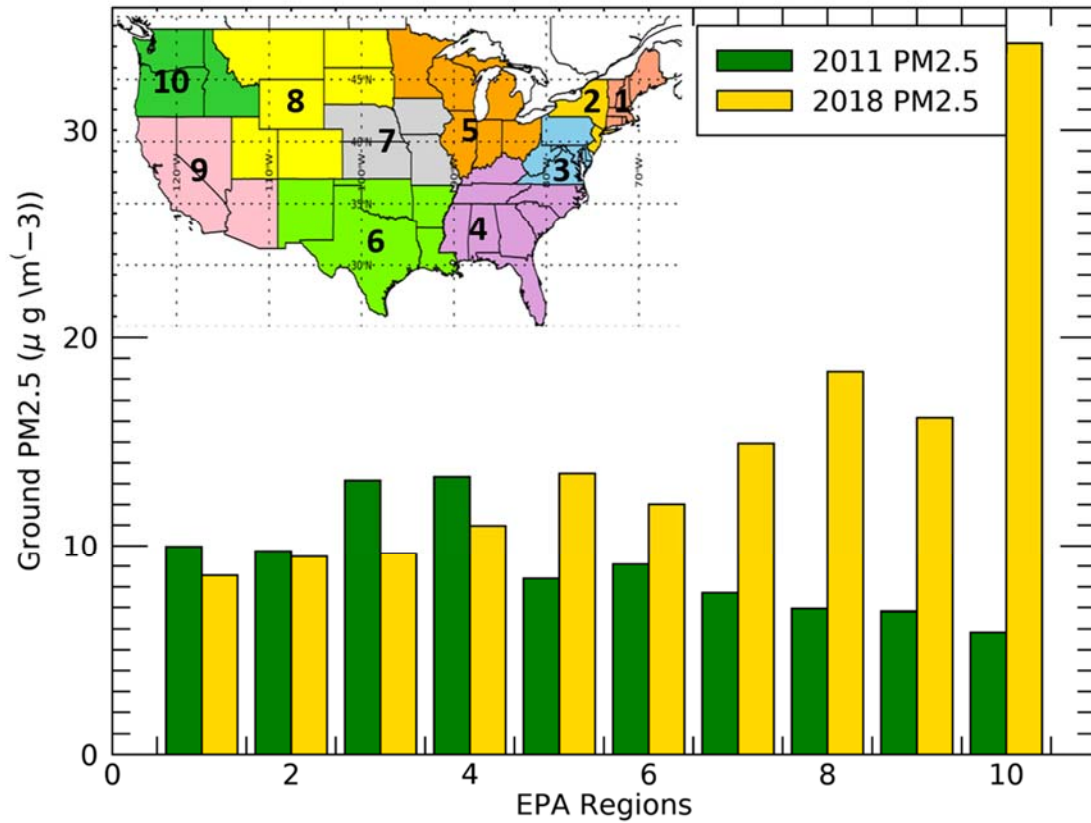
725

726

Figure 5. Mean PM_{2.5} from August 9th to August 25th in 2018 and 2011 of most affected states

727

728



729

730 Figure 6. Mean PM_{2.5} of EPA regions from August 9th to August 25th in 2011 and 2018. Inset
731 shows the map of 10 EPA regions in different colors. Yellow column represents the 2018 mean
732 PM_{2.5} and green column represents for 2011 mean PM_{2.5}.

733

734